Adsorption of atomic and molecular oxygen on 3C-SiC(111) and ([overline 1][overline 1][overline 1]) surfaces: A first-principles study

Junjie Wang, Litong Zhang, Qingfeng Zeng, Gerard L. Vignoles, Laifei Cheng, Alain Guette

Adsorption of atomic and molecular oxygen on 3C-SiC(111) and $(\bar{1}\bar{1}\bar{1})$ surfaces: a first principles study

Junjie Wang[1*], Litong Zhang[1], Qingfeng Zeng[1], Gérard L. Vignoles[2], Laifei Cheng[1], and Alain Guette[2]

[1] National Key Laboratory of Thermostructure Composite Materials,

Northwestern Polytechnical University, Xi'an 710072, P. R. China

[2] Laboratory for Thermostructural Composites, UMR 5801, CNRS-CEA-Snecma-Université

Bordeaux l, F-33600 Pessac, France

Density-functional theory calculations were performed to investigate the adsorption of oxygen on the 3C-SiC(111) and $(\bar{1}\bar{1}\bar{1})$ surfaces, including single O atom, double O atoms and variable oxygen coverage adsorptions. We find that the Bridge (BR) and On-Top (OT) sites are the most stable adsorption sites for the (111) and $(\bar{1}\bar{1}\bar{1})$ surfaces, respectively. According to the 2D PES achieved, the lowest continuous oxygen diffusion path over the whole surface seems to be BR→H3→BR→BR(neighbor)→etc. By studying the double O atoms adsorption on 3C-SiC(111) surface, we find that 2-BR is the most favorable configuration. By comparing adsorption energies and O-O distances with reference values, we get that there is an electronic induction effect, which helps to get a more stable adsorption structure, between neighboring O adatoms with small amount of negative charge, which favors a medium O-O distance. Spin-unrestricted first principles molecular dynamics calculations have been carried out to achieve more dynamic information and comprehensive understanding of the molecular oxygen adsorption on a 3C-SiC(111) surface. The results confirm our determined diffusion path and one of the preferred double atoms configuration. By studying the adsorption of oxygen at 3C-SiC(111) and $(\bar{1}\bar{1}\bar{1})$ surfaces as a function of oxygen coverage, we find that the adsorption energy initially increases (1/9-3/9 ML (MonoLayer)) then significantly decreases (3/9-6/9 ML) with increasing oxygen coverage and finally reaches a stable value (7/9-1.0 ML) for 3C-SiC(111) surface. For 3C-SiC $(\bar{1}\bar{1}\bar{1})$ surface, the trend is similar to the (111) surface case, however the variation is small when the oxygen coverage is above 3/9 ML and the adsorption energy at 1/9 ML coverage is lower. By combining the results of adsorption energy, structure evolution and electronic density difference calculations, we get that the total adsorption energy is determined by the interaction between adatoms and by surface reconstructions: attractive (resp. repulsive) interactions between adatoms make the adsorption structure more (resp. less) stable, *i.e.* it gets a larger (resp. smaller) adsorption energy; however, surface reconstructions can eliminate the stress caused by repulsive interactions between adatoms and make the adsorption structure to be stable.

I. INTRODUCTION

Silicon carbide is a Ⅳ-Ⅳ compound material showing many excellent properties: low density, high strength, low thermal expansion, high thermal conductivity, high elastic modulus, superior chemical inertness, wide band gap and large electron mobility [1]. Therefore, it is promised to be widely used in high-temperature and high-power applications, such as hot-section structural components of gas turbines, heat exchanger tubes for industrial furnaces [2] and high temperature, high power, and high frequency electronic devices and sensors [3]. When silicon carbide is used as thermal structure material, it can be oxidized in the working environment. On

the contrary, silicon carbide designed for electronic applications is intentionally oxidized during processing to form a thin layer of SiO_2. The oxidation of SiC is therefore an important issue in practically all its applications.

Accordingly, the oxidation of silicon carbide surfaces has attracted much attention as one of the most important processes in current and future SiC technology.

Scientifically, a precise control of the surface oxidation or an improvement of its oxidation-resistance require detailed knowledge of the initial reactions of oxygen with SiC surfaces on atomic scale. Many groups have extensively studied chemical reactions at SiC surfaces and subsequent oxidation processes by using various experimental techniques such as X-ray photoelectron spectroscopy (XPS) [4], surface X-ray diffraction (SXRD) [5], reflection high energy electron diffraction (RHEED) [6], high resolution electron energy loss spectroscopy (HREELS) [7, 8], low-energy electron diffraction (LEED)[9, 10], electron energy loss (EELS) spectroscopies [4], scanning tunneling microscopy (STM) [11, 12], photoemission spectroscopy using synchrotron radiation (SRPS) [9, 13, 14], high-resolution medium energy ion scattering (MEIS) [15], resonant reaction profiling (NRP) techniques [16], high resolution photoelectron spectroscopy (HRPS) [17], scanning tunneling spectroscopy (STS) [12] and so on. The initial chemisorption of oxygen on SiC single crystal surfaces has also correspondingly been the subject of intensive theoretical research [18-20]. In Ref. [18], studies of O adsorption on clean and H-saturated Si-rich 3C-SiC(001) 3×2 surfaces within density functional theory are presented. Déak *et al* [19] determined by first principles calculations that the most likely reaction routes in the oxidation process produces carbon interstitials at the interface. A three-oxygen cluster analogous to the well-known “thermal donor” in Si was observed by Ventra *et al* [20] in their first-principles calculations. However, atomic structures of oxide complexes and initial oxidation processes even at submonolayer coverage remain not fully understood yet, especially for 3C-SiC(111) surfaces that are technologically relevant.

In this paper, we examine the relative stability of adsorption sites, the diffusion of oxygen atom, the interaction between adsorbed oxygen atoms, and the influence of oxygen coverage, on the 3C-SiC(111) (Si-terminated) and $(\bar{1}\bar{1}\bar{1})$ (C-terminated) surfaces in the context that it may provide some insight into the oxidation behavior of 3C-SiC.

The paper is organized as follows. In Sec. II, we briefly describe the building of 3C-SiC(111) and $(\bar{1}\bar{1}\bar{1})$ surface models and address the calculation method. In Sec. III A, we report our results on the adsorption of a single O atom on 3C-SiC(111) and $(\bar{1}\bar{1}\bar{1})$ surfaces. In particular, we obtain the energy surface of O atom adsorption by investigating conceivable O reaction pathways on 3C-SiC(111) surface from initial sites through transition states on the path to the corresponding final adsorption sites . In Sec. III B, the adsorption of oxygen atom pairs on 3C-SiC(111) surface has been investigated. We also present spin-unrestricted first principles molecular dynamics simulations to investigate the adsorption process of a dioxygen molecule. In Sec. III C, adsorption of oxygen on 3C-SiC(111) and $(\bar{1}\bar{1}\bar{1})$ surfaces as a function of oxygen coverage has been studied. A short summary concludes the paper in Sec. IV.

II. MODEL BUILDING AND CALCULATION FRAMEWORK

The SiC surface model (illustrated in Fig. 1) in the present calculations employs the usual slab-supercell geometry, to which periodic boundary conditions are applied. An infinite stack of quasi-2D slabs is generated from this. Each slab is separated from its neighbors by a certain vacuum width. The thickness of a slab is usually expressed in terms of a number of atomic layers, where a layer is defined as a (111) plane that contains Si or C atoms. The thickness of a slab and the width of the vacuum layer can affect the surface energy of the surface model. Therefore, we firstly present the effects of these variables on the surface energy to determine the model parameters. Calculations have been performed for slab thicknesses of three to fifteen layers, and a variety of different vacuum widths. The surface energy, $E_{surf}(n, L)$, for a system comprising n layers and a vacuum width of L can be defined as:

$$E_{surf}(n,L) = \frac{E_{tot}(n,L) - E_{tot}(n,0)}{A} \qquad (1)$$

where $E_{tot}(n,L)$ and A are the total energy and total surface area per repeated unit, respectively. L=0 corresponds to the bulk crystal. Since each slab has two surfaces, A is twice the area of each surface per repeated unit.

For slab thickness of 8 layers, the convergence of $E_{tot}(n, L)$ (shown in Fig. 2(a)) as vacuum width L tends to infinity is clear. Figure 2(b) shows the dependence of $E_{tot}(n, L)$ on slab thickness, for a vacuum width of 10Å. The convergence to the infinite limit is also quite rapid. Based on these surface energy calculations, we build the 3C-SiC (111) and $(\bar{1}\bar{1}\bar{1})$ surface models (illustrated in Fig. 1) with a periodic supercell containing a vacuum width of 20Å and a slab consisting of 12 layers of Si(C) atoms with a 3×3 lateral unit cell (9 primitive surface cells per supercell). Calculated and experimental lattice parameters for 3C-SiC are given in Table I. The 3C-SiC parameters achieved from our GGA-PW91 calculation is adopted for our slab construction. In addition, each broken sp_3 bond at the bottom layer atoms in each supercell is saturated with one hydrogen atom. The lowest three layers of atoms were kept fixed in order to hold the characteristics of a more realistic surface, while the rest of the unit cell was allowed to relax during the geometry optimizations.

Four adsorption sites are considered in our work. Figure 3 shows different O adsorption configurations, which are : (i) a single-coordinated “On Top” site (OT in the following), (ii) a twofold-coordinated “Bridge” site (BR in the following), (iii) a threefold-coordinated “Hollow” site (H3 in the following) and (iv) a fourfold-coordinated site (T4 in the following).

The adsorption energies can be calculated using the following equation:

$$\Delta E_{ads} = \left(\frac{N}{2} E(O_2) + E(\text{total}) - E(\text{slab}) \right) / N \qquad (2)$$

where N is the number of O atoms adsorbed on the SiC surface, E(slab) and E(total) are the calculated total energies of the surface with and without oxygen, respectively. $E(O_2)$ is the total energy of an isolated dioxygen molecule. The calculations of oxygen atom(s) adsorptions are based on the density functional theory (DFT) code DMOL3 [22, 23] from Accelrys. The electronic settings involved in the tests are shown in Table II. In these tests, the single point energies of the 3C-SiC(111) surface model have been calculated.

According to the result of tests, the DND basis set, which is comparable to the Gaussian 6-31G*

basis sets, and the Perdew-Wang approximation [24] (GGA-PW91) are used in our calculations. The real space cutoff radius is of 4.0 Å. All-electron basis sets are used for all the elements. A Fermi smearing of 0.01 hartree is employed to improve computational performance. The convergence criteria for energy, gradient, and displacement are respectively 2×10^{-5} hartree, 4×10^{-3} hartree/Å, and 5×10^{-3} hartree/Å. Accurate Brillouin zone sampling is ensured by summing over a finite set of k-points chosen according to the Monkhorst-Pack scheme with a grid spacing of 0.05 $Å^{-1}$ (*i.e.* a 3×3×1 k-point setting). The convergence tests in the *k*-points sampling and electronic Hamiltonian are illustrated in Fig. 4. From Fig. 4, we can get that a 'medium quality' setting with 3×3×1 k-points are accurate enough for the calculations on our models.

To determine the activation barrier for the O atom diffusion among adsorption sites, the complete linear synchronous transit (LST) and quadratic synchronous transition (QST) [25] search methods are employed, followed by transition state confirmation through the nudged elastic band (NEB) method[26].

III. RESULTS AND DISCUSSION

A. Adsorption of single oxygen atom on 3C-SiC (111) and $(\bar{1}\bar{1}\bar{1})$ surfaces

In this section we present investigations on the adsorption of a single O atom on the 3C-SiC (111) and $(\bar{1}\bar{1}\bar{1})$ surface models. The four optimized adsorption sites on the 3C-SiC(111) surface are shown in Fig. 5. On the other hand, OT (Fig. 6) is the only equilibrium adsorption site on the 3C-SiC $(\bar{1}\bar{1}\bar{1})$ surface. The calculated adsorption energies and structural parameters for these adsorption sites are listed in Table III.

On the 3C-SiC(111) surface, therefore, chemisorption of O atom was found to be strongly exothermic, and the BR adsorption site is the most stable one. By comparing the lengths and electronic populations of Si-O bonds (Table III), the Si-O bond of the OT site (see Fig. 5) was found stronger than others. The BR site, however, was found to be the most stable chemisorption site. This configuration could be regarded as a siloxane function, *i.e.* the precursor of the Si-O-Si rings of silicon dioxide, which is the product of SiC oxidation. It corresponds to the usual bivalent bonding state of oxygen, with the octet rule being satisfied; the small Si-O-Si angle (with respect to sp_3 hybridization) may result from lone electron pair repulsion, as in H_2O, and is associated to a Si-Si distance shrinking, as seen in Fig. 5. The lower energy value of OT with respect to BR is rather expected, because the surface Si atoms are unable to form a true double bond with oxygen.

One of the interesting results emerging from the calculations is that the adsorption energies of O atoms on the H3 and T4 sites are smaller than those of BR and OT sites. These two sites exhibit threefold symmetry, as illustrated in Fig. 6, which guarantees zero lateral forces for the adsorbed O atoms. From a conventional guess [28], these high-symmetry sites could be more favored than the other ones, in contradiction with our results. However, the large coordination number of these sites brings an excess of valence electrons, so there is obviously an anti-bonding character, not present in OT or BR. In accordance with this, the Si-O bond populations and the Mulliken charges for O are neatly smaller (Table III) on the high-symmetry sites. The T4 site is further disfavored because of the close vicinity of the underlying C atom (Table IV), which reinforces the

anti-bonding contribution. From the calculation results, we can guess that one of the Si-O bonds of H3 or T4 structure can be easily broken up under some disturbance and an H3 to BR or a T4 to BR transition is possible.

In order to complete these results, the surface migration events of an oxygen adatom have been investigated by calculating the energy barriers to be overcome when jumping between different adsorption locations.

By means of the NEB method [28], we were able to find the minimum energy path (MEP) connecting the initial and final states of each migration step. The highest maximum along the MEP defines the energy barrier. The initial and final states correspond to the optimized adsorption geometries obtained before. The energy barriers of oxygen atom migration between adsorption sites on 3C-SiC(111) surface are listed in Table V. The computed values indicate that the migrations from T4 to BR and OT sites are activated with a barrierless channel. This result reveals that the T4 site is not stable: it can be considered as a transition state between BR sites. This is not in contradiction with the former results, since the preceding method was not allowing any lateral movement of the T4 oxygen atom with respect to its vertical path coinciding with the symmetry axis. So, T4 is actually a saddle point on a dynamical point of view.

Diffusion of the O atom to a BR site from an OT site (1.018 eV) is more difficult than from an H3 site (0.433 eV) because of the stronger Si-O bond of OT site adsorption. However, an OT site adatom may be moved to a BR site by some strong environmental disturbance, for example the electronic repulsion from another O adatom. The energy barriers between OT and H3 sites are quite high, *i.e.* the migration between these two sites is difficult. The energy barriers for oxygen atom diffusion from BR to OT, H3 and T4 sites are 1.186, 0.635 and ≥1.269 eV, respectively. And a 1.100 eV energy barrier should be overcome for an oxygen atom jump between two neighboring BR sites. Therefore, we can get that the movements of O atom from BR to OT and to T4 are more difficult than to H3 because of higher energy barriers. As a summary, the lowest continuous path over the whole surface seems to be BR→H3→BR→BR(neighbor)→etc…as shown in Fig. 7, which is a graphical representation of an approximate 2D PES, illustrating the stability islands and the lowest energy paths. Note that T4 appears indeed as a "hilltop" here, confirming it s lack of stability with respect to horizontal movements.

On the 3C-SiC $(\bar{1}\bar{1}\bar{1})$ surface, the computed oxygen adsorption energy at OT site is 1.724 eV (Table III), which is 2.092 eV smaller than the O adsorption energy at OT site on 3C-SiC (111) surface. Therefore, we can get that the 3C-SiC $(\bar{1}\bar{1}\bar{1})$ (C-terminated) surface is less oxygen activated than the 3C-SiC (111) (Si-terminated) surface, which is consistent with the results of former experimental and theoretical studies [28, 29] that the oxygen atoms prefer to adsorb on cation terminated semiconductors (such as GaN, AlN *et al*) surfaces.

B. Adsorption of oxygen atom pairs on 3C-SiC (111) surface

Our studies indicate that BR site is the most stable "single O atom" adsorption (i.e. with a surface coverage of 1/9 ML) site on 3C-SiC(111) surface, while the OT site adsorption structure has the strongest Si-O bond. However, the O atom adsorption structure and energetics could be different in presence of a neighboring O adatom. Therefore, studying the oxygen adsorption with

larger oxygen atom coverages is important and necessary. In this section, we present a systematic investigation of the adsorption of oxygen atom pairs on the 3C-SiC(111) surface. By considering the relative positions of oxygen atoms, the size of our unit cell (9 elementary cells) and the periodicity condition at boundaries, we have built 32 possible combinations of adsorption sites, which are illustrated in Fig. 8. After geometry optimization, 13 stable configurations (4 kinds: 2BR, 2OT, OT-H3 and BR-OT) were obtained (see Fig. 9). The detailed structure parameters, adsorption energies and evolutions of oxygen atom pairs are listed in Table VI.

By studying the evolution of adsorption configurations, we find that all T4 site and most of the H3 sites (except in OT-H3 configurations) involved in these initial configurations were converted to BR sites. So, it seems that the T4 and H3 are not stable adsorption sites for the adsorption of oxygen atom pair : the repulsion from neighboring oxygen atom pushes the T4 or H3 oxygen atoms away from their initial sites. On the contrary, all OT sites involved keep their positions, as well as most of 2BR configurations (except 2BR-(2) and -(3) became to 2BR-B and –A, respectively). All those results are consistent with our study about single O atom diffusion barriers in last section.

Fig. 10 is a comparison of the adsorption energies (Fig. 10) of the most stable configurations of each kind, taking the adsorption energies of single O atoms as reference energies. The reference energies of 2BR, 2OT, OT-H3 and BR-OT configurations are E_{BR}, E_{OT}, $1/2(E_{OT}+E_{H3})$, and $1/2(E_{BR}+E_{OT})$, respectively. E_{BR}, E_{OT}, and E_{H3} represent the single O atom adsorption energies on BR, OT and H3 sites. Since each layer has 9 atoms in our surface model, the oxygen coverages for single and double O atoms adsorptions can be regarded as 1/9 and 2/9 ML, respectively. It appears that 2-BR is the most favorable adsorption configuration.

Figure 11 reports the double-site configuration energies as a function of the shortest O-O distance. For the 2BR configurations (Fig. 11(a)), there is an optimal disposition in which the shortest O-O distance is about 4 Å. For the 2OT configurations (Fig. 11(b)), the adsorption energy increases with the shortest O-O distance: the largest O-O distances are favored. For the OT-H3 configurations (Fig. 11(c)), the adsorption energies firstly become smaller and then increase. For the BR-OT configurations (Fig. 11(d)), the adsorption energies have a more complex evolution, with a global tendency to increase except a decrease around 4.5 A.

Figure 12 illustrates the initial relative positions of neighboring adatoms for oxygen atom pairs adsorption on 3C-SiC (111) surface. For both BR and OT-center conditions, Fig. 12 shows that there always is a “void” region (a circular region) with no neighbor. For the central BR site, its stable neighboring sites (including neighboring BR and OT sites) with a small adsorption energy loss (in red) from twice the single-atom value lie on the small circle or outside the larger circle, and the other BR sites having an extra adsorption energy (in green) lie in the region between two circles. Similarly, the central OT site has two neighboring “energy-gained” H3 sites (in green) lie in medium distance, and the neighboring “energy-loss” sites lie on the smaller hexagon and circle or on the larger hexagon circle.

From these calculation results, we can conclude that the adsorption of oxygen favors low coverage situations, similarly to what has been found for GaN [28, 30]. However, in some cases,

the adsorption of oxygen favors a moderate O-O distance of about 3 to 4 Å: these are the 2BR-A, B and C and the OT-H3-A configurations, whose adsorption energies are larger than those reference energies. From Table VI, we also see that the optimized O-O distance is smaller than the reference distance only for those configurations. This reveals that there are some electronic effects between the O adatoms, and the electronic effects are related with the O-O distance (between 3 and 4 Å) and oxygen adatom charge $q(O) \leq 0.95e$.

The reason for the qualitatively different behavior of the different kinds of configurations can be understood in terms of the surface adsorption structures (Fig. 6) on different adsorption sites. Oxygen has a higher electronegativity than silicon atom (the electronegativity of O and Si are respectively 3.44 and 1.9) [30], and therefore, the Si–O bonds formed at the surface are strongly polarized towards the O atom making it a negatively charged ion. For OT site adsorption structure, the Si-O bond distance is 1.573 Å. Consequently, there is almost no screening between the negatively charged O adatoms of 2OT configurations and a strong repulsive electrostatic interaction results when they are close to each other. For the 2BR and OT-H3 configurations, the oxygen atoms at BR and H3 site relax into the surface layer (at 1.193 Å and 1.133 Å above the Si layer at BR and H3 sites, respectively), therefore, resulting in a smaller electrostatic repulsion between the oxygen adatoms. In some situations (a medium O-O distance), another effect may further reduce the repulsive interaction or even help to produce a small attractive interaction between adatoms.

To find out the nature of this electronic effect, we consider the difference electron density of each configuration. "Difference Electron Density" is typically the difference between the actual DFT computed electron density and an assumed standard or model electron density. It can be used to represent the electron redistribution after reactions of atoms to molecule or atoms assembly. Hence, people can interpret chemical bonding by drawing electron density difference maps.

As an example, the contour plot (through a plane containing the O adatoms) of difference densities for single O atom BR site adsorption and five 2BR adsorption configurations are shown in Fig. 13. In almost all cases, the nonbonding electron density seems to lie perpendicularly (on the z axis projection) to the siloxane bond axis: it is close to a classical AX_2E_2 Gillespie hybridization scheme. For 2BR-B (Fig. 13(c), the O-O distance is 4.063 Å), the electron clouds of adatoms are connected above the neighboring Si atom. *i.e.* the non-bonding hybrid orbital of the Si atom lying between the two siloxane functions provides a weak bridge connecting the non-bonding orbitals of the oxygen atoms, as shown in Fig. 14. Thus, the attractive interaction between O adatoms of 2BR-B configuration should originate from this weak bonding. For 2BR-C (Fig. 13(d), the O-O distance is 3.686 Å), the connection between the electron clouds of adatoms is not formed, however, the connecting of O atom (lower of Fig. 13(d)) and two neighboring Si atoms could also strengthen the surface adsorption structure. For 2BR-D (Fig. 13(e), the O-O distance is 2.768 Å), there is a dramatic decrease of electron density between the two adatoms. This reveals that the direct interaction between oxygen adatoms is repulsive. For 2BR-A and E configurations, the difference electron densities (Fig. 13(b) and (e)) are not enough to explain the adsorption energies, however, the electron contribution in these two figures are similar which is consistent with the adsorption energy calculations that these two configurations have close adsorption energies. In 2BR-E, the situation is similar to 2BR-B except that the angles are not the same: the oxygen orbitals are all aligned. This may provide some antibonding character. In 2BR-A, the hybrid AOs of the siloxane oxygens are also parallel, though staggered. This situation

is rather similar to 2BR-C, where each oxygen is weakly bonded to a neighboring Si not lying between the two sites, but here they are closer to each other, so that the direct repulsion exerted in 2BR-D is already present.

Hence, we can conclude that there are electronic induction effect, which helps to get a more stable adsorption structure, between neighboring O adatoms without large amounts of charge (less than 0.95e in present work). This kind of electronic induction effect demands a medium O-O distance: 3-4 Å, a particular relative orientation of the two adatoms, and a participation of some Si surface atom placed in between the adatoms.

In order to achieve more dynamic information and comprehensive understanding of the molecular oxygen adsorption on 3C-SiC(111) surface, we also carried out first principles molecular dynamics calculations in this section.

Three spin-unrestricted FPMD calculations have been performed on a system containing an oxygen molecule placed 3.5 Å above the 3C-SiC(111) surface, with the O-O axis perpendicular to the surface over different sites (OT, H3 and T4 sites). In all cases, the molecule is initially at rest. The observed chemisorption paths are characterized by a number of common features which are independent of the initial positions. A time step of 1 fs is used in all molecular dynamic simulations, which are performed in the NVE ensemble. The NVE ensemble (also known as the microcanonical ensemble) is obtained by solving the standard Newton equations of motion without any pressure and temperature control. Energy is conserved when this (adiabatic) ensemble is generated. In the present work, we are interested in exploring the constant energy surface of the conformational space, and we do not want the perturbation introduced by temperature bath coupling. Therefore, we adopt the NVE ensemble instead of NVT ensemble. Before launching the O_2 molecule, the clean 3C-SiC(111) surface is equilibrated at a temperature of 273 K for 500 fs.

The case of an O_2 molecule placed perpendicularly above a T4 site is illustrated in Figs. 15-17. Figure 15 shows the evolution of local temperature and O-O distance during the simulation. Once the dynamic procedure starts, the molecule is spontaneously attracted towards the surface, and the O-O distance remains stable before adsorption. The Coulomb force from the electron-deficient top Si atoms steers the molecule in the direction of the most favorable adsorption site (Fig. 16(a)-(d))- i. e., a top Si atom which has a dangling bond. The O-O bond dissociates as a consequence of this process, the O-O distance increasing abruptly in a way which indicates a nonthermal, “hot-atom” mechanism that takes place *e. g.* during the chemisorption of O_2 on Al(111)[32], TiN(001)[33], Si(001)[34] and other metal surfaces [35]. Namely, in the simulation shown in Fig. 15, the O-O distance increases from 1.707 Å to 4.395 Å in 60 fs of simulated time, which corresponds to an initial mean velocity of 2.24×10^3 m/s per atom. Therefore, the kinetic energy of the “hot” atoms after the dissociation (Fig. 16(g)) is high enough to push the OT site oxygen atom over the energy barrier between OT and BR sites (Fig. 7). The oxygen atoms diffuse on the 3C-SiC(111) surface along the BR->H3->BR->BR(neighbor) path, which is consistent with the diffusion path achieved in the last section. After what we could call a fast structural optimization, the final configuration (Fig. 16(o)) is 2BR-C: the second most energetically favored among all. Later on, the two O atoms remain trapped in these two sites with a very little oscillation. As shown in Fig. 15, a sudden increase in the local temperature up to ~680 K is induced after the dissociation. The total adsorption energy of 2BR-C configuration is 8.111 eV, which can be regarded as the heat source of the increase of local temperature from initial 273 K to final about 600 K.

According to molecular orbital theory, the molecular orbital of O_2 can be presented as $O_2[KK(\sigma 2s)^2(\sigma^* 2s)^2(\sigma 2p_x)^2(\pi 2p_y)^2(\pi 2p_z)^2(\pi^* 2p_y)^2(\pi^* 2p_z)^2]$. Figure 17 shows the evolution of the local density of states projected onto the O atoms during the adsorption of molecular oxygen on the 3C-SiC(111) surface. From the gradual sinking of the LUMO peak below the Fermi level, we infer that the increasing donation of electrons from the surface into the π^* antibonding orbitals of the molecule can be used to characterized the adsorption process, as pointed out in Ref. [34].

C. Adsorptions of oxygen on 3C-SiC(111) and $(\bar{1}\bar{1}\bar{1})$ surfaces with different coverages

Our studies in Sec. III A have shown that BR and OT are the most stable adsorption sites on 3C-SiC(111) and $(\bar{1}\bar{1}\bar{1})$ surfaces, respectively. We calculated the adsorption energies for various oxygen coverage values: 1/9, 2/9, 3/9, 4/9, 5/9, 6/9, 7/9, 8/9 and 1 ML (monolayer), at these two adsorption sites.

Our results for the O adsorption structures are shown in Fig. 18. The calculated highest adsorption energies as a function of O-coverage for both (111) and $(\bar{1}\bar{1}\bar{1})$ surfaces are shown in Fig. 19. The positive adsorption energies shown in Fig. 19 suggest that the reactions between the O atoms and the surface atoms are exothermic, especially for (111) surface. On the 3C-SiC(111) surface, all oxygen atoms preferentially adsorb on BR sites (Fig. 18), and the adsorption energy increases from 3.984 eV at 1/9 ML coverage to 4.116 eV at 3/9 ML (Fig. 19), indicating strong attractive interactions between the three adatoms. The difference electron densities are given in Fig. 20. It can be seen that there is a high electron density region in the center of 3 adatoms (*i.e.* on the Si atom which is surrounded by three O atoms) at 3/9 ML coverage (Fig. 20 (a)). The region connects these three adatoms and shows that there is a weak bonding among the adatoms, similar to what we have discussed before for 2BR-B..

The adsorption energy significantly decreases for coverages greater than 4/9 ML, which indicates that a strong repulsive interaction between adsorbates builds up. At that moment, low electron density regions (Fig. 20(b)) appear between the adatoms, indicating repulsive interactions between the O adatoms in accordance with the decrease in adsorption energy. With the increase of oxygen coverage, the repulsive interaction between adsorbates becomes stronger: the difference electron densities of 6/9 and 1.0 ML are shown in Fig. 20(c) and (d) as examples.

However, the adsorption energy decreases slowly for coverages greater than 5/9 ML, indicating that there is a new factor to counteract the effect of increasing repulsive interaction on O adsorption energy. From our optimized structures (Fig. 18), we can find that when the oxygen coverage is above 5/9 ML, significant surface reconstructions occur. At 6/9 ML coverage, the Si-C bonds are still preserved, however Si and C atoms of the top two layers displace away from their symmetrical positions. At 7/9 ML coverage, the strong displacement of the Si and C atoms lead to the breaking of some Si-C bonds of the first two layers and the formation of strengthened Si-O bonds and some C-C bonds. When 1 ML O atoms cover all the BR sites at the surface, these O adatoms and surface Si atoms form an Si-O bilayer. The formation of this Si-O bilayer breaks the Si-C bonds underneath, making the surface C bind themselves to only three Si atoms: two with the surface Si and one with a Si in the next SiC bilayer. Consequently, the significant surface reconstructions can eliminate the stress caused by repulsive interactions between adatoms and make the adsorption structure more stable.

For the 3C-SiC $(\bar{1}\bar{1}\bar{1})$ surface, similar with the condition of (111) surface, the magnitude of the adsorption energies firstly increases from 1.724 eV at 1/9 ML coverage to 1.883 eV at 3/9 ML coverage and then decrease to 1.793 eV at 1.0 ML coverage, but the variation is small when the oxygen coverage is above 3/9 ML, indicating a weak attractive interaction.

To gain more insight into the nature of the bonding, we consider the difference electron density (Fig. 21). The three-dimensional, real-space plots of difference electron densities for oxygen OT site on 3C-SiC $(\bar{1}\bar{1}\bar{1})$ for variation oxygen coverages (Fig. 21) show that (i) there are binding interactions which contribute to the increase of oxygen adsorption energies, between adatoms of 2/9, 3/9 and 4/9 ML coverage values (Fig. 21(b), (c) and (d)); (ii) with the increase of oxygen coverage, these interactions between adatoms were weakened, and the shape and magnitude of the difference electron density distributions are very similar for 5/9, 6/9, 7/9, 8/9 and 1.0 ML, indicating a similar bond nature.

The reason for the qualitatively different behavior at the 3C-SiC $(\bar{1}\bar{1}\bar{1})$ surface can be explained by noticing that the electronegativity difference between C and O atoms is less than that between Si and O atoms (the electronegativities of O, C and Si are respectively 3.44, 2.6 and 1.9) [30]. Our studies in Sec. III A reveal that the charge amount of O atom at OT site on 3C-SiC $(\bar{1}\bar{1}\bar{1})$ surface is -0.38 $|e|$ (Table III), which is a quite small quantity comparing with that of O atom (q(O)=-0.95$|e|$) at BR site on 3C-SiC(111) surface. Therefore, according to the conclusion of Sec. III B, there is always an electronic attractive effect between neighboring O adatoms till 1.0 ML coverage, hence, the adsorption energy of 1/9 ML coverage is lower than those of other situations.

IV. SUMMARY

We have carried out first principles calculations to investigate the adsorption of atomic and molecular oxygen on 3C-SiC(111) and $(\bar{1}\bar{1}\bar{1})$ surface. First, in order to get the most favorable adsorption site, the single oxygen atom adsorptions on four different sites (BR, OT, H3 and T4) have been studied. By comparing the magnitude of adsorption energies of different sites, we get that Bridge (BR) site, which can be regarded as the precursor of the Si-O rings of silicon dioxide, is the most favorable one. On the 3C-SiC $(\bar{1}\bar{1}\bar{1})$ surface, however, OT is the only one stable site. By means of the NEB method, the energy barriers of diffusion pathway between adsorption sites on (111) surface have been studied. An approximate 2D PES, which illustrates the stability islands and the lowest energy paths, is also achieved. According to the 2D PES, the lowest continuous oxygen diffusion path over the whole surface seems to be BR→H3→BR→BR(neighbor)→etc… Also, the T4 site is confirmed as unstable.

In the next section, we presented a systematical investigation for the adsorption of oxygen atom pairs on the 3C-SiC(111) surface. After structural optimizations, 4 kinds of configurations have been confirmed (2BR, 2OT, H3-OT and BR-OT). By studying the evolution of adsorption

configurations, we found that all T4 sites and most of H3 sites (except H3 sites in OT-H3 configurations) involved in these initial configurations were converted to BR sites. By comparing the calculation results of adsorption energies, we get that 2-BR is the most favorable configuration. We have also studied the effect of a neighboring oxygen atom on the adsorption energies of O adatoms by comparing the results of single atom and atom pair adsorptions. From the calculation results, we conclude that for the 2-OT and BR-OT configurations the adsorption of oxygen could favor low coverage situation. However, for the 2-BR and OT-H3 configurations, the adsorption of oxygen favors a moderate O-O distance of about 3 to 4 Å. To achieve more dynamic information and comprehensive understanding of the molecular oxygen adsorption on 3C-SiC(111) surface, a series of spin-unrestricted first principles molecular dynamics calculations have been carried out. The oxygen atoms diffuse along the BR→H3→BR→BR(neighbor) path, which is consistent with the diffusion path achieved in Sec. III B. The final configuration is one of the most stable among the previously found ones. By studying the O-O distance evolution, we find that a "hot-atom" mechanism controls the O_2 dissociation process. By studying the local density of states projected onto the O atoms during the adsorption of molecular oxygen on 3C-SiC(111) surface, we find that the dissociation adsorption of O_2 on 3C-SiC(111) surface in the adiabatic limit is triggered by partial filling of the antibonding molecular orbital of dioxygen due to hybridization with the surface states.

In Sec. III C, adsorptions of oxygen at BR and OT sites on 3C-SiC(111) and $(\bar{1}\bar{1}\bar{1})$ surfaces with different coverage values have been studied. We find that the adsorption of oxygen at the 3C-SiC(111) surface has a larger binding energy than at the $(\bar{1}\bar{1}\bar{1})$ surface. The trend of the adsorption energy as a function of the oxygen coverage for the 3C-SiC(111) surface is: the adsorption energy initially increases (1/9-3/9 ML) then significantly decreases (3/9-6/9 ML) with increasing of oxygen coverage and finally reaches a stable value (7/9-1.0 ML). The difference electronic density calculation result reveals that there is an attractive interaction between adatoms for 2/9 and 3/9 ML coverages, however, when oxygen coverage reaches 4/9 ML, the repulsive interaction between adatoms builds up. Then, because of significant surface reconstructions, the adsorption energy does not continue to decrease with increasing coverage beyond 6/9 ML. For the 3C-SiC $(\bar{1}\bar{1}\bar{1})$ surface, similar with the situation of (111) surface, the adsorption energy initially increases (1/9-3/9 ML) then decreases (3/9-1.0 ML) with increasing of oxygen coverage, however the variation is small when the oxygen coverage is above 3/9 ML and the adsorption energy at 1/9 ML coverage is the lowest. By combining the results of adsorption energy and difference electronic density calculations, it is found that there is always attractive interaction, which reaches maximum at 3/9 ML coverage and then decreases with increasing of oxygen coverage, between adatoms.

The provided results are hopefully a valuable input for the construction of a kinetic model of the first steps of SiC surface oxidation.

ACKNOWLEDGEMENT

The authors acknowledge financial support from Snecma Propulsion Solide under contract FPR

No. 0539298A.. We also thank Northwestern Polytechnical University High Performance Computing Center for allocation of computing time on their machines.

*Electronic address: pro_junjie@yahoo.com.cn

[1]H. Morkoc, S. Strite, G. B. Gao, M. E. Lin, B. Sverdlov, and M. Burns, J. Appl. Phys. **76**, 1363 (1994).

[2]N. S. Jacobson, J. Am. Ceram. Soc. **76**, 3 (1993).

[3]M. A. Capano, R. J. Trew, Mater. Res. Soc. Bull. **22**, 19 (1997).

[4]V. M. Bermudez, J. Appl. Phys. **66**, 6084 (1989).

[5]W. Voegeli, K. Akimoto, T. Urata, S. Nakatani, K. Sumitani, T. Takahashi, Y. Hisada, Y. Mitsuoka, S. Mukainakano, H. Sugiyama, X. Zhang, H. Kawata, Surf. Sci. **601**, 1048 (2007).

[6]X. Xie, K. P. Loh, N. Yakolev, S. W. Yang and P. Wu, J. Chem. Phys. **119**, 4905 (2003).

[7]J. A. Schaefer and W. Göpel, Surf. Sci. **155**, 535 (1985).

[8]H. Ikeda, K. Hotta, T. Yamada, S. Zaima, and Y. Yasuda, Jpn. J. Appl. Phys. Part 1 **34**, 2191 (1995).

[9]C. Virojanadara and L. I. Johansson, Surf. Sci. **505**, 358 (2002).

[10]C. Virojanadara and L. I. Johansson, Phys. Rev. B **71**, 195335 (2005).

[11]D. G. Cahill and Ph. Avouris, Appl. Phys. Lett. **60**, 326 (1992).

[12]H. Ikegami, K. Ohmori, H. Ikeda, H. Iwano, Sh. Zaima, and Y. Yasuda, Jpn. J. Appl. Phys., Part 1 **35**, 1593 (1996).

[13]F. Amy, P. Soukiassian, Y. K. Hwu and C. Brylinski, Phys. Rev. B **65**, 165323 (2002).

[14]P. Soukiassian and F. Amy, J. Electron Spectrosc. **144-147**, 783 (2005).

[15]Y. Hoshino, R. Fukuyama and Y. Kido, Phys. Rev. B **70**, 165303 (2004).

[16]C. Radtke, I. J. R. Baumvol, B.C. Ferrera and F. C. Stedile, Appl. Phys. Lett. **85**, 3402 (2004).

[17]D. Schmeiβer, D. R. Batchelor, R. P. Mikalo, P. Hoffmann and A. Lloyd-Spetz, Appl. Surf. Sci. **184**, 340 (2001).

[18]E. Wachowicz, R. Rurali, P. Ordejón and P. Hyldgaard, Comp. Mater. Sci. **33**, 13 (2005).

[19]A. G. P. Déak, J. Knaup, Z. Hajnal, Th. Frauenheim, P. Ordejón, J.W. Choyke, Physica B **340-342**, 1069 (2003).

[20]M. Di Ventra and S. T. Pantelides, Phys. Rev. Lett. **83**, 1624 (1999).

[21]*Physics of Group IV Elements and III-V Compounds*, edited by O. Madelung *et al*., Landolt-Börnstein, New Series, Goup II, Vol. 17a (Springer, Berlin, 1982).

[22]B. Delley, J. Chem. Phys. **92**, 508 (1990).

[23]B. Delley, J. Chem. Phys. 113, 7756 (2000).

[24]J. P. Perdew, J. A. Chevary, S. H. Vosko, K. A. Jackson, M. R. Pederson, D. J. Singh, C. Fiolhais, Phys. Rev. B, **46**, 6671 (1992).

[25]N. Govind, M. Petersen, G. Fitzgerald, D. King-Smith and J. Andzelm, Comp. Mater. Sci. **28** 250 (2003)

[26]G. Henkelman and H. Jonsson, J. Chem. Phys. **113**, 9901 (2000).

[27]B. M. Rice, L. M. Raff, and D. L. Thompson, J. Chem. Phys. **88**, 7221 (1988).

[28]Q. Sun, A. Selloni, T. H. Myers, and W. A. Doolittle, Phys. Rev. B **74**, 195317 (2006).

[29]H. Ye, G. Chen, Y. Zhu, and S. H. Wei, Phys. Rev. B **77**, 033302 (2008).

[30]T. K. Zywietz, J. Neugebauer, and M. Scheffler, Appl. Phys. Lett. **74**, 1695 (1999).

[31]G. Aylward and T. Finlay, SI Chemical Data, 3rd ed. (Wiley, Singapore, 1994).

[32]L. C. Ciacchi and M. C. Payne, Phys. Rev. Lett. **92**, 176104 (2004).

[33]S. Piscanec, L. C. Ciacchi, E. Vesselli, G. Comelli, O. Sbaizero, S. Meriani, and A. DeVita, Acta Mater. 52, 1237 (2004).
[34]L. Colombi Ciacchi and M. C. Payne, Phys. Rev. Lett. 95, 196101 (2005).
[35]J. Wintterlin, R. Schuster, and G. Ertl, Phys. Rev. Lett. 77, 123 (1996).

TABLE CAPTIONS

TABLE I. Lattice parameters of 3C-SiC from experiments [21] and present calculations.

TABLE II. The electronic Hamiltonian settings involved in the convergence tests.

TABLE III. The adsorption energies, O-Si distances, overlap populations in the Si-O bond region and O atom Mulliken charges for the different adsorption configurations of single oxygen atom on 3C-SiC(111) and 3C-SiC ($\bar{1}\bar{1}\bar{1}$) surfaces.

TABLE IV. Detailed bond parameters of OT, BR, H3, and T4 adsorption structures of single oxygen atom on 3C-SiC(111) surface.

TABLE V. The energy barriers for oxygen atom diffusion between adsorption sites on 3C-SiC(111) surface.

TABLE VI. The detailed structure parameters, adsorption energies and evolutions for the double oxygen atoms adsorption on the 3C-SiC(111) surface.

TABLE I. Lattice parameters of 3C-SiC from experiments [21] and present calculations.

Source	Lattice constant (Å)	Interlayer distance (Å)	Bond length (Å)	Err. (%)
Expt.	**4.360**	**1.090**	**1.88794**	**0**
Calc. (LDA-PWC)	4.335	1.084	1.87704	-0.577
Calc. (LDA-VWN)	4.334	1.083	1.87662	-0.600
Calc. (GGA-PW91)	**4.384**	**1.096**	**1.89829**	**0.548**
Calc. (GGA-PBE)	4.385	1.096	1.89878	0.574

TABLE II. The electronic Hamiltonian settings involved in the convergence tests.

Quality	Functional	SCF tolerance (Hartree)	Core treatment	Basis set	Orbital cutoff (Å)
Coarse	GGA-PW91	1×10^{-4}	All electron	DN	3.5
Medium	GGA-PW91	1×10^{-5}	All electron	DND	4.0
Fine	GGA-PW91	1×10^{-6}	All electron	DNP	4.6

TABLE III. The adsorption energies, O-Si distances, overlap populations in the Si-O bond region and O atom Mulliken charges for the different adsorption configurations of single oxygen atom on 3C-SiC(111) and 3C-SiC ($\bar{1}\bar{1}\bar{1}$) surfaces.

	3C-SiC (111)				3C-SiC ($\bar{1}\bar{1}\bar{1}$)			
	E_{ads} (eV)	$d_{O\text{-}Si}$ (Å)	pop[$d_{O\text{-}Si}$] (|e|)	q(O) (|e|)	E_{ads} (eV)	$d_{O\text{-}C}$ (Å)	pop[$d_{O\text{-}C}$] (|e|)	q(O) (|e|)
OT	3.816	1.573	0.88	-1.03	1.724	1.283	0.83	-0.38
BR	3.984	1.795	0.48	-0.95	unstable	-	-	-
H3	3.782	1.953	0.33	-0.85	unstable	-	-	-

T4	2.715	2.075	0.26	-0.82	unstable	-	-	-

TABLE IV. Detailed bond parameters of OT, BR, H3, and T4 adsorption structures of single oxygen atom on 3C-SiC(111) surface.

Structure	Bond	Distance (Å)	Population
OT	O-Si1	1.573	0.88
	O-C1(2, 3)	2.935	-0.10
BR	O-C1(2)	2.833	-0.12
	O-C3	2.429	-0.29
	O-Si1(3)	1.795	0.48
	O-Si2	2.786	0
	Si1-Si3	2.589	-0.36
H3	O-C1(2, 3)	2.560	-0.22
	O-Si1(2, 3)	1.953	0.33
T4	O-C1	2.286	-0.41
	O-Si1(2, 3)	2.075	0.26

TABLE V. The energy barriers for oxygen atom diffusion between adsorption sites on 3C-SiC(111) surface.

Initial position	Final position	Energy barrier(eV)
T4	OT	0
T4	BR	0
OT	T4	≥1.100
OT	H3	1.285
OT	BR	1.018
H3	OT	1.250
H3	BR	0.433
BR	BR	1.100
BR	OT	1.186
BR	H3	0.635
BR	T4	≥1.269

TABLE VI. The detailed structure parameters, adsorption energies and evolutions for the double oxygen atoms adsorption on the 3C-SiC(111) surface.

Final configuration		Initial configuration	Adsorption energy (eV/atom)		O-O distance (Å)	
			2 O atoms adsorption	Reference energy	Optimized distance	Reference distance
2BR	A	2BR-(1); 2BR-(3); T4-H3-(3); BR-T4 -(1);	4.006	3.984	3.051 4.069 3.686	3.071 4.106 3.714
	B	2BR-(2); 2BR-(4); 2H3-(2); 2T4-(1)	4.063		2.768	2.714
	C	2BR-(5); T4-H3-(2); BR-T4-(2); BR-T4-(3); BR-T4-(4);	4.056			
	D	H3-BR-(2); H3-BR-(4) 2BR-(6)	3.862		5.342	5.322
	E	2BR-(7); 2H3-(1); 2T4-(2); T4-H3-(1); H3-BR-(1)	3.917			
BR-OT	A	BR-OT-(1)	3.822	3.900	3.108	2.970
	B	BR-OT-(2)	3.733		3.055	2.443
	C	BR-OT-(3); OT-T4-(2)	3.863		4.438	4.226
	D	BR-OT-(4); OT-T4-(1)	3.820		4.649	4.636
2OT	A	2OT-(1)	3.775	3.816	5.329	5.298
	B	2OT-(2)	3.619		3.694	3.082
OT-H3	A	OT-H3-(1)	3.818	3.799	3.395	3.612
	B	OT-H3-(2)	3.736		4.763	4.731

FIGURE CAPTIONS

FiG. 1. Side and top views of 3C-SiC (111) ((a) and (c)) and $(\bar{1}\,\bar{1}\,\bar{1})$ ((b) and (d)) surfaces. In this and all following figures related to the surface structure, black, gray and white spheres respectively indicate oxygen silicon and hydrogen atoms.

FIG. 2. The variation of surface energy as a function of (a) vacuum thickness and (b) slab thickness. The slab thickness in (a) is 8 layers, and the vacuum thickness for (b) is 10Å.

FIG. 3. Schematic atomic structures of O atom adsorption sites on the 3C-SiC(111) surface (3C-SiC $(\bar{1}\,\bar{1}\,\bar{1})$ surface adsorption sites structure could be obtained by exchanging the positions of Si and C atoms). In this and all following figures related to the surface structure, red spheres indicate oxygen atoms.

FiG. 4. The variation of total energy of 3C-SiC(111) surface model as a function of *k*-points setting at different electronic parameters settings (coarse, medium and fine).

FIG. 5. Top and side views of the optimized possible O atom adsorption sites on the 3C-SiC(111) surface. Dashed lines represent repulsions between atoms which have same kind of charge.

FIG. 6. Top and side views of the optimized O atom adsorption site (OT) on the 3C-SiC $(\bar{1}\,\bar{1}\,\bar{1})$ surface.

FIG. 7. Approximate 2D PES of oxygen atom diffusion on 3C-SiC(111) surface, interpolated from the energies of the sites and transition states; The stars indicate the locations of the transition states. The Green line with arrows represents a lowest-energy continuous diffusion path.

FIG. 8. Possible configurations of double oxygen atoms adsorption on 3C-SiC(111) surface.

FIG. 9. Optimized configurations of double oxygen atoms adsorption.

FIG. 10. Adsorption energy for double O atoms on 3C-SiC(111) surface as a function of adsorption configuration.

FIG. 11. The variation of adsorption energies of double O atoms on 3C-SiC(111) surface as a function of O-O shortest distance. Dot lines indicate the reference adsorption energies. (a) 2BR configuration; (b) 2-OT configuration; (c) OT-H3 configuration; (d) BR-OT configuration.

FIG. 12. FIG. 12. Neighboring stable adsorption sites around given BR and OT sites adatoms for oxygen atom pairs adsorption on 3C-SiC (111) surface. These dashed circles and hexagons are guides to eyes.

FIG. 13. Contour plot (through a plane containing the O adatoms marked in the figure and parallel to (111) surface) of difference electron densities for single O atom (a) and double O atoms (b-f) adsorption structures at BR site on 3C-SiC(111) surface.

FIG. 14. Scheme of the inter-siloxane bridging in 2BR-B configuration. The empty circle around the central Si atom is a vertical hybrid AO.

FIG. 15. Evolution of local temperature and O-O distance during FPMD simulation of the oxygen molecular chemisorption reaction.

FIG. 16. Snapshots from FPMD simulation of the dissociative adsorption of molecular oxygen on the 3C-SiC(111) surface. The arrows indicate the moving directions of oxygen atoms. (a) Initial

configuration (simulation time t=0); (b) t=200 fs; (c) t=500 fs; (d) t=500 fs; (d) t=556 fs; (e) t=587 fs; (f) t=665 fs; (g) t=685 fs; (h) t=725 fs; (i) t=745 fs; (j) t=767 fs; (k) t=805 fs; (l) t=845 fs; (m) t=875 fs; (n) t=916 fs; (o) final configuration t=1000 fs.

FIG. 17. Evolution of the local density of states projected onto the O atoms during the adsorption of molecular oxygen on 3C-SiC(111) surface (left) and correspondent snapshots (right) from a FPMD simulation started with the molecule perpendicular to the surface over a T4 site. The vertical line indicates the Fermi level. The continuous and dashed lines indicate the O 2s and 2p states, respectively, (a) Initial configuration (t=0 fs); (b) Adsorption (t=554 fs); (c) Dissociation (t=664 fs); (d) Final configuration (t=1000 fs)

FIG. 18. Top and side view of optimized structures of O adsorption at the BR site of the 3C-SiC(111) surface and OT site of the 3C-SiC $(\bar{1}\,\bar{1}\,\bar{1})$ at various O coverages.

FIG. 19. Adsorption energies per oxygen adatom as a function of oxygen coverage. (a) Oxygen adsorptions on 3C-SiC(111) surface; (b) Oxygen adsorptions on 3C-SiC $(\bar{1}\,\bar{1}\,\bar{1})$ surface.

FIG. 20. Contour plot (through a plane containing the O adatoms marked in the figure) of difference electron densities for coverages of 3/9 (a), 4/9 (b), 6/9 (c), and 1.0 ML (d) on 3C-SiC(111) surface.

FIG. 21. Three-dimensional real-space contour plots of difference electron densities for O OT site on 3C-SiC $(\bar{1}\,\bar{1}\,\bar{1})$ for coverages of 1/9 (a), 2/9 (b), 3/9 (c), 4/9 (d), 5/9 (e), 6/9 (f), 7/9 (g), 8/9 (h) and 1.0 ML (i). The value of the isospheres of (a), (b), (d) and (d) are $1\times10^{-3}e$/ Å^3; the value of the isospheres of (e), (f), (g), (h) and (i) are $1\times10^{-5}e$/ Å^3.

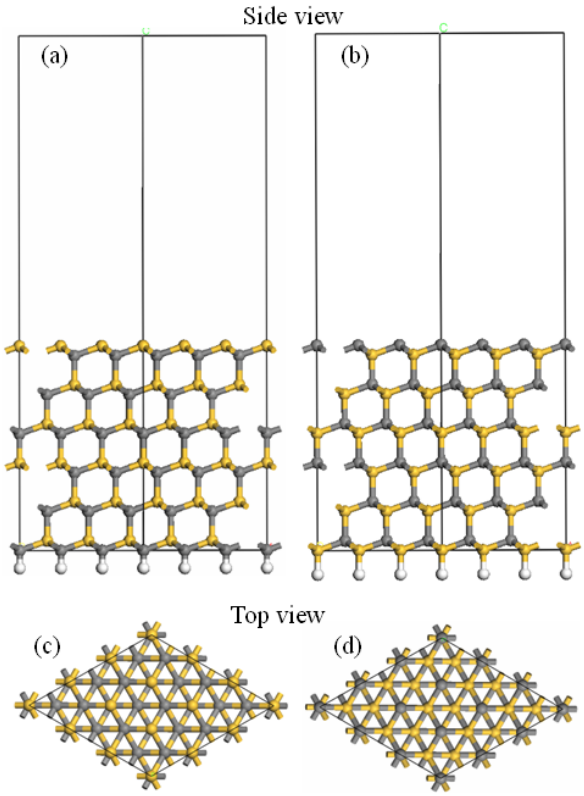

FiG. 1. Side and top views of 3C-SiC (111) ((a) and (c)) and $(\bar{1}\,\bar{1}\,\bar{1})$ ((b) and (d)) surfaces. In this and all following figures related to the surface structure, black, gray and white spheres respectively indicate oxygen silicon and hydrogen atoms.

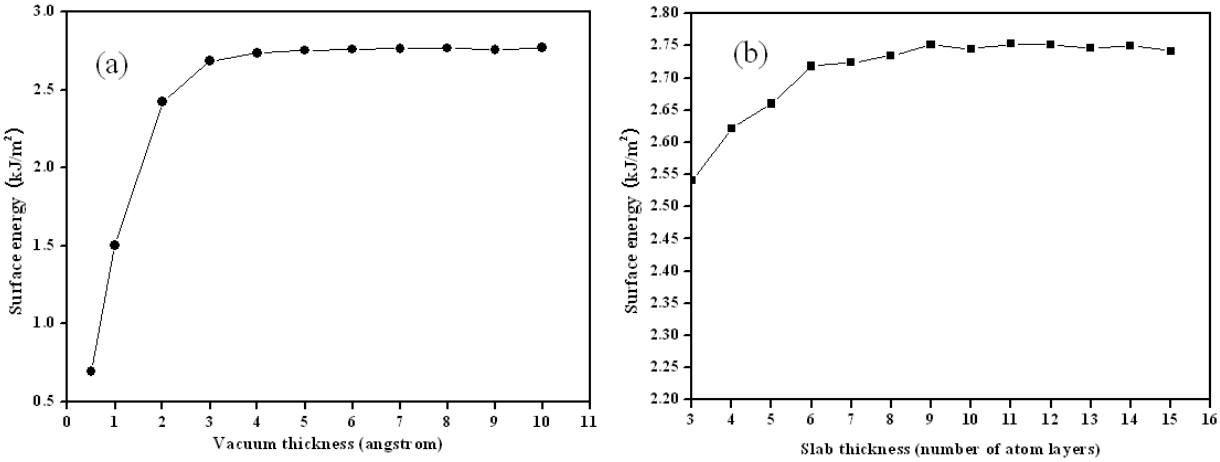

FIG. 2. The variation of surface energy as a function of (a) vacuum thickness and (b) slab thickness. The slab thickness in (a) is 8 layers, and the vacuum thickness for (b) is 10Å.

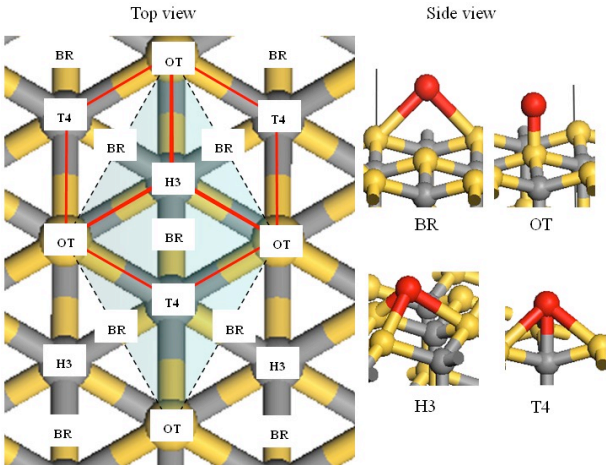

FIG. 3. Schematic atomic structures of O atom adsorption sites on the 3C-SiC(111) surface (3C-SiC $(\bar{1}\,\bar{1}\,\bar{1})$ surface adsorption sites structure could be obtained by exchanging the positions of Si and C atoms). In this and all following figures related to the surface structure, red spheres indicate oxygen atoms.

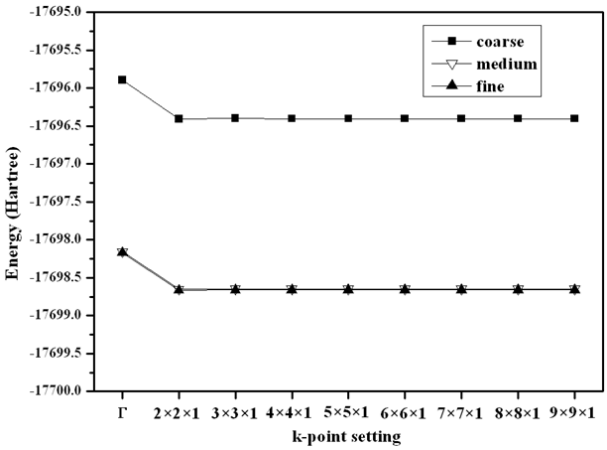

FiG. 4. The variation of total energy of 3C-SiC(111) surface model as a function of *k*-points setting at different electronic parameters settings (coarse, medium and fine).

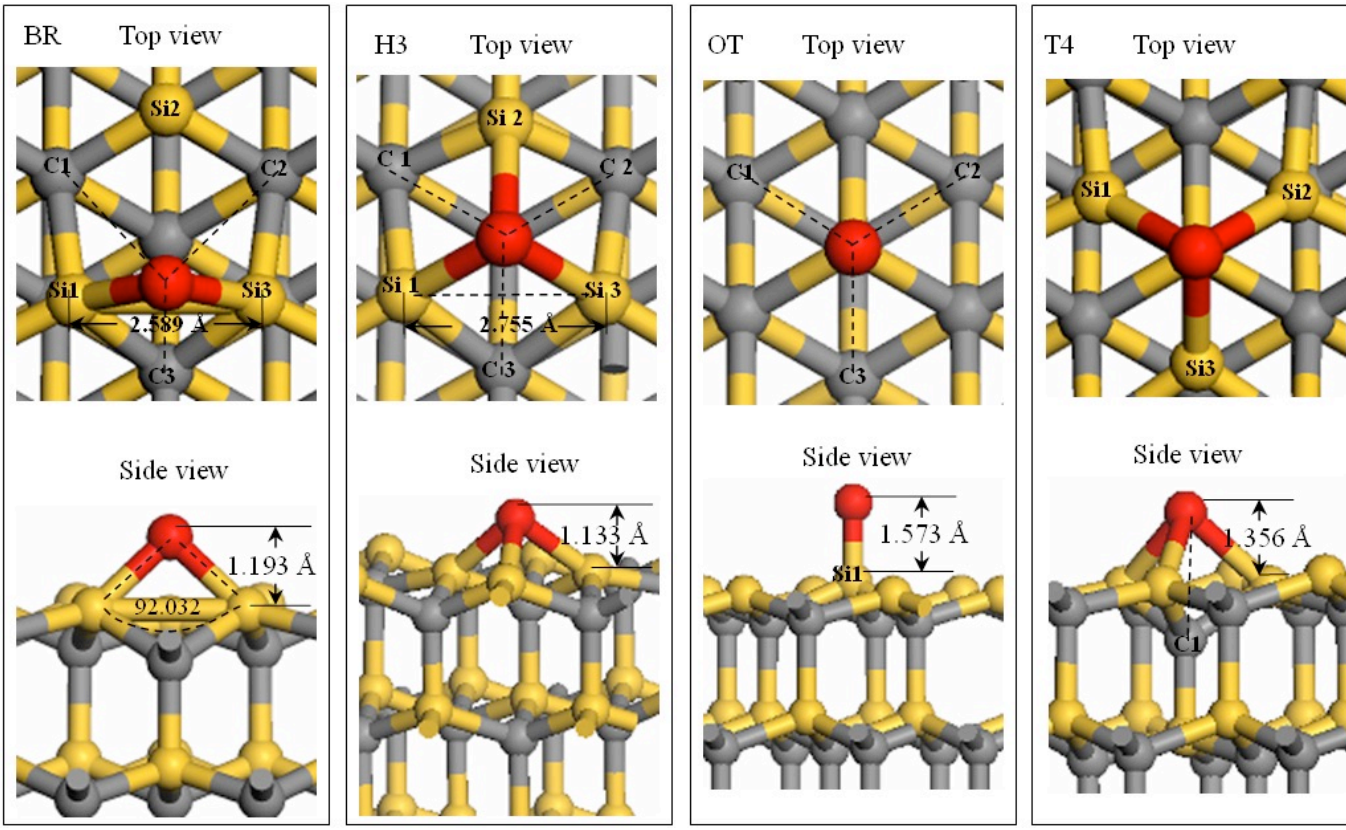

FIG. 5. Top and side views of the optimized possible O atom adsorption sites on the 3C-SiC(111) surface. Dashed lines represent repulsions between atoms which have same kind of charge.

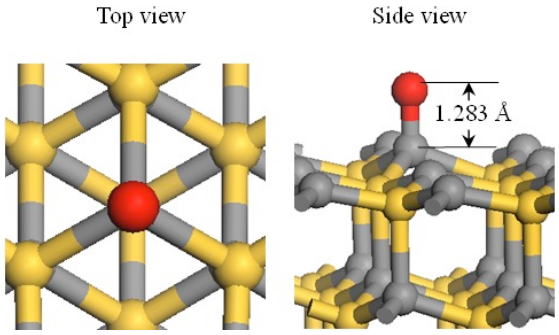

FIG. 6. Top and side views of the optimized O atom adsorption site (OT) on the 3C-SiC $(\bar{1}\,\bar{1}\,\bar{1})$ surface.

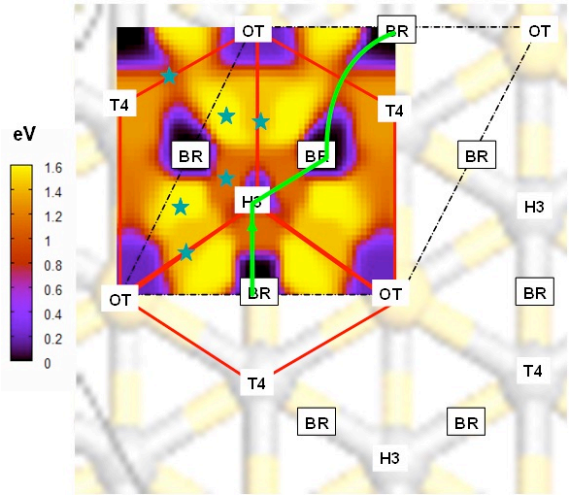

FIG. 7. Approximate 2D PES of oxygen atom diffusion on 3C-SiC(111) surface, interpolated from the energies of the sites and transition states; The stars indicate the locations of the transition states. The Green line with arrows represents a lowest-energy continuous diffusion path.

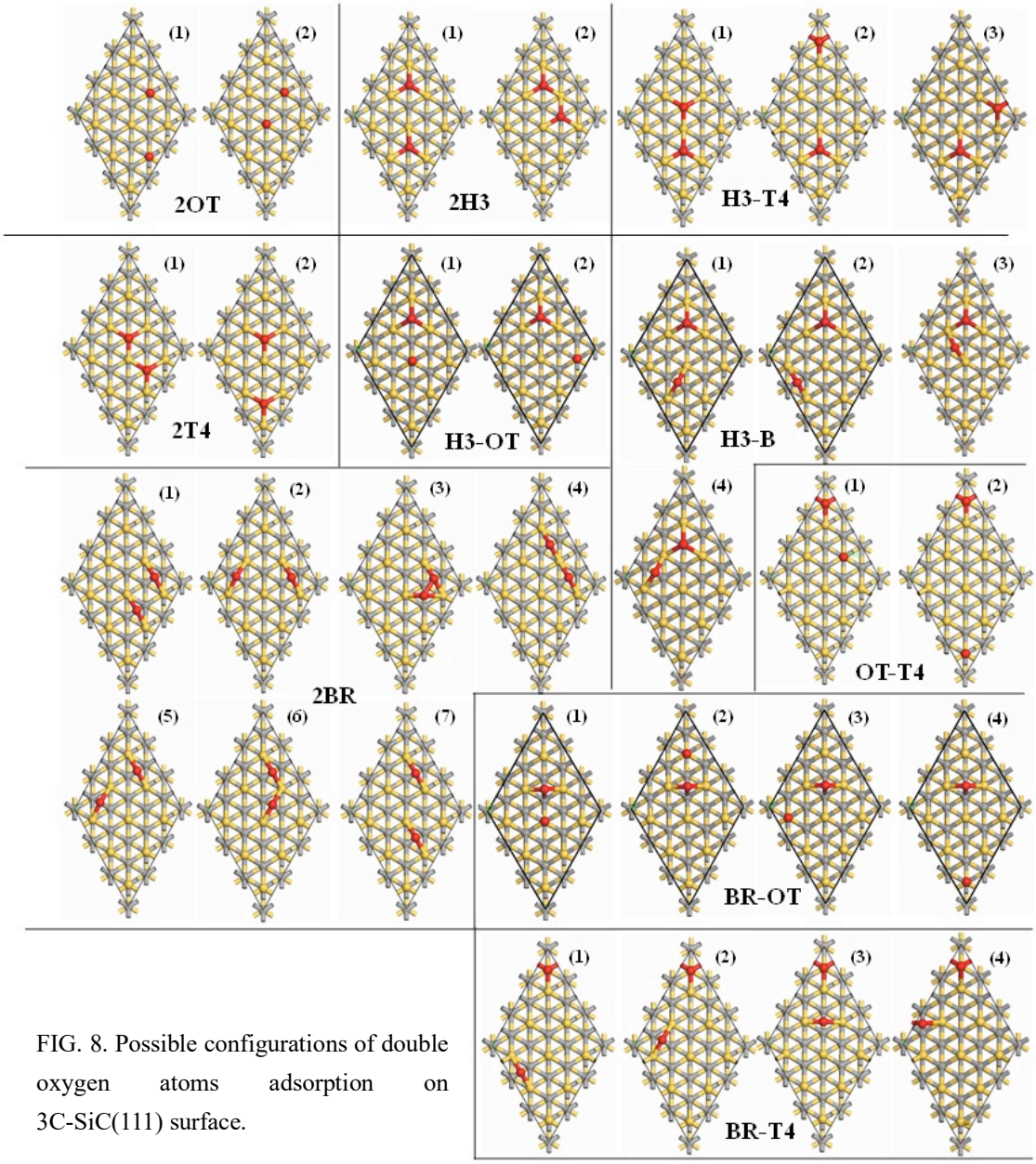

FIG. 8. Possible configurations of double oxygen atoms adsorption on 3C-SiC(111) surface.

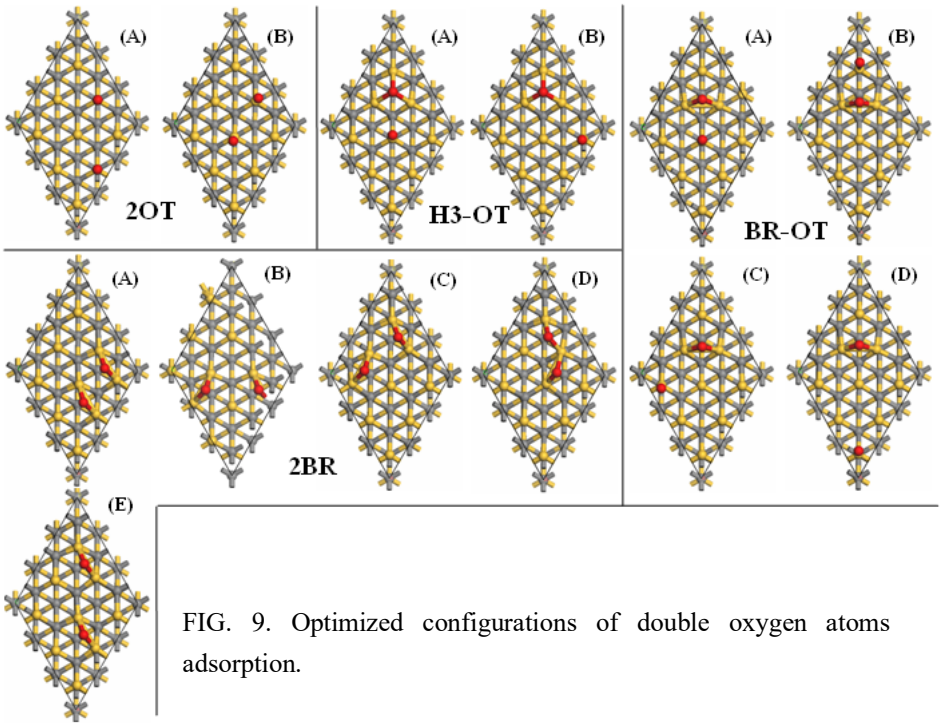

FIG. 9. Optimized configurations of double oxygen atoms adsorption.

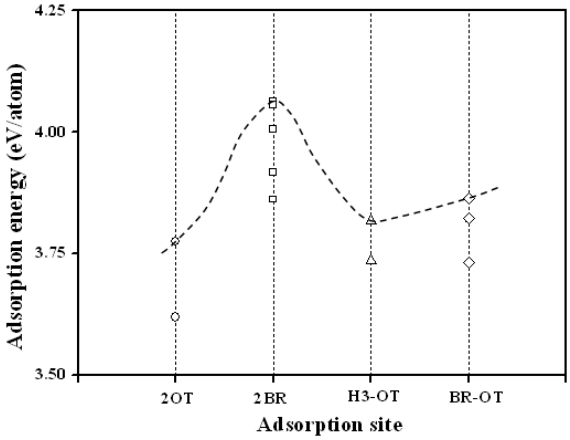

FIG. 10. Adsorption energy for double O atoms on 3C-SiC(111) surface as a function of adsorption configuration.

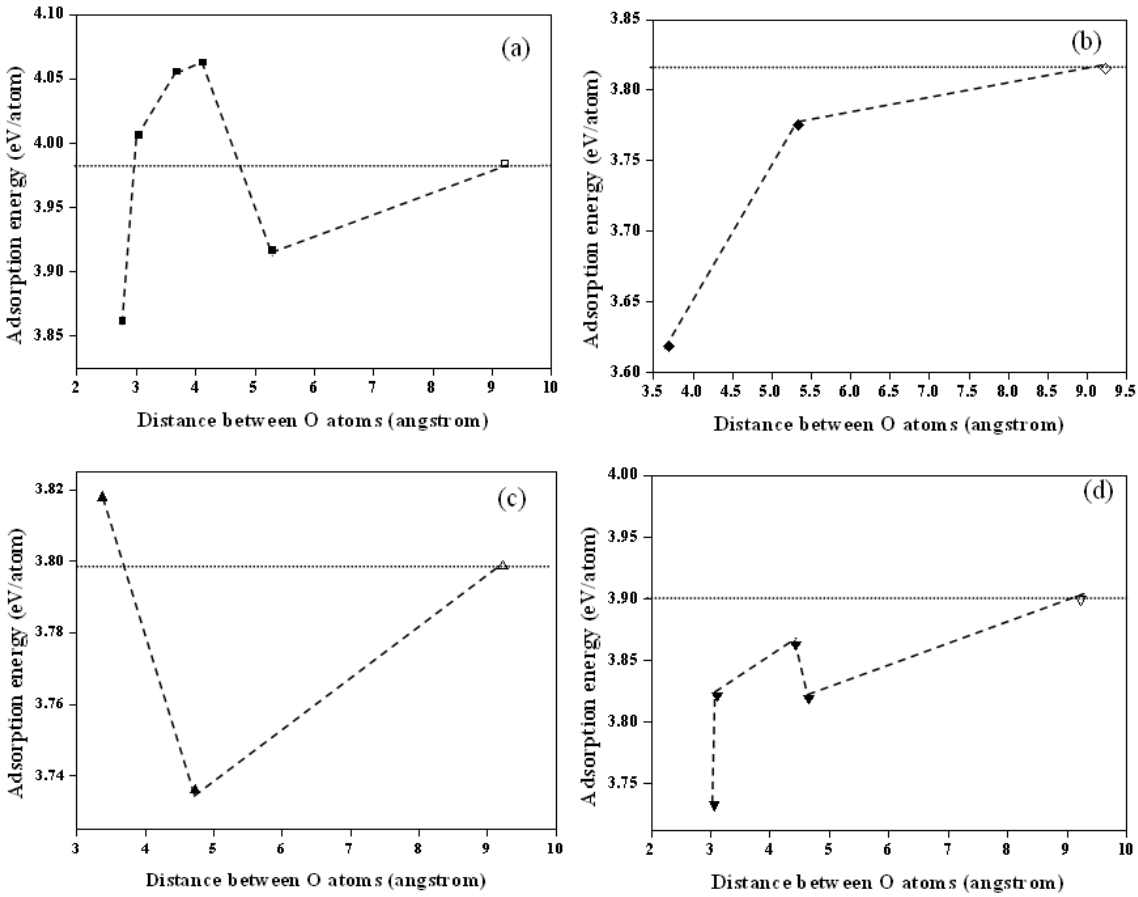

FIG. 11. The variation of adsorption energies of double O atoms on 3C-SiC(111) surface as a function of O-O shortest distance. Dot lines indicate the reference adsorption energies. (a) 2BR configuration; (b) 2-OT configuration; (c) OT-H3 configuration; (d) BR-OT configuration.

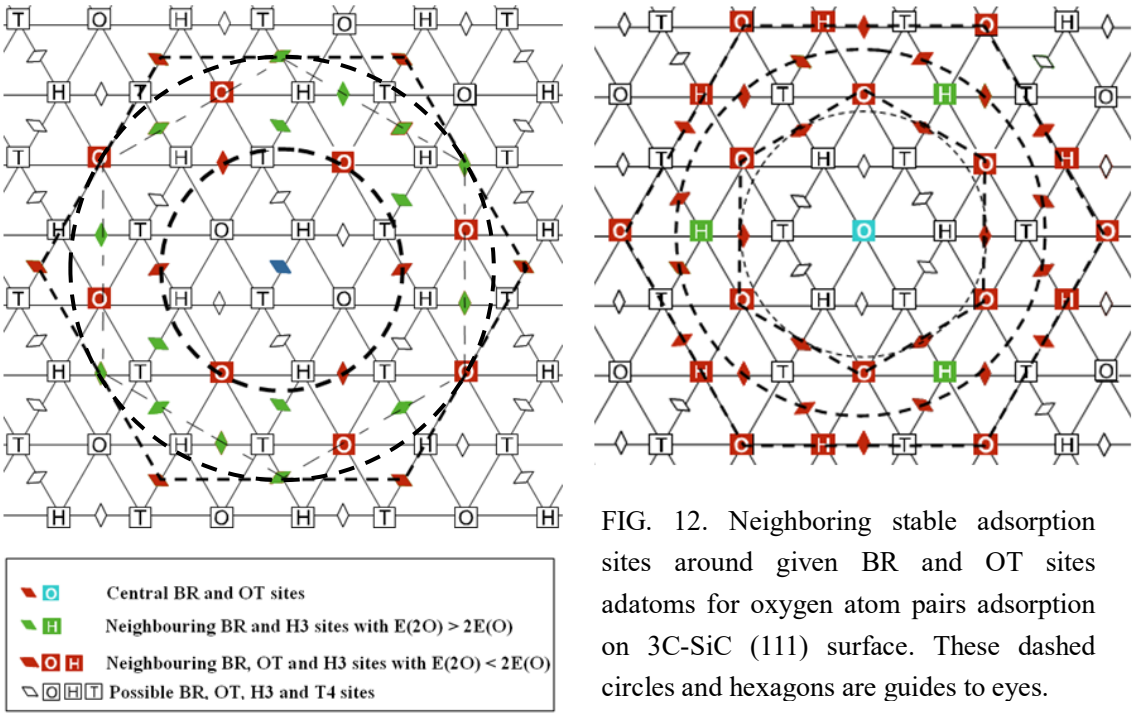

FIG. 12. Neighboring stable adsorption sites around given BR and OT sites adatoms for oxygen atom pairs adsorption on 3C-SiC (111) surface. These dashed circles and hexagons are guides to eyes.

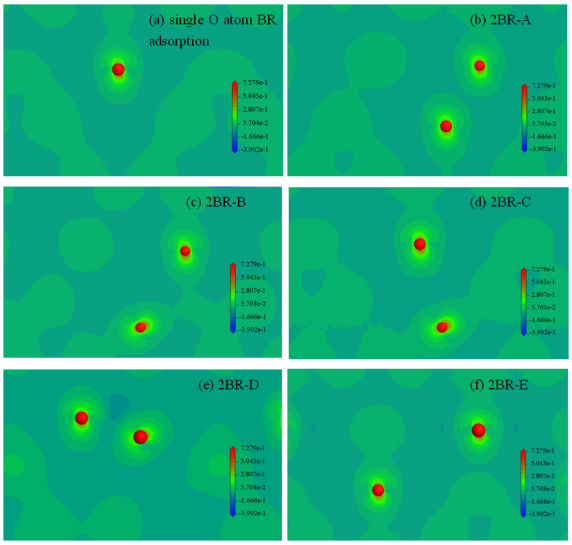

FIG. 13. Contour plot (through a plane containing the O adatoms marked in the figure and parallel to (111) surface) of difference electron densities for single O atom (a) and double O atoms (b-f) adsorption structures at BR site on 3C-SiC(111) surface.

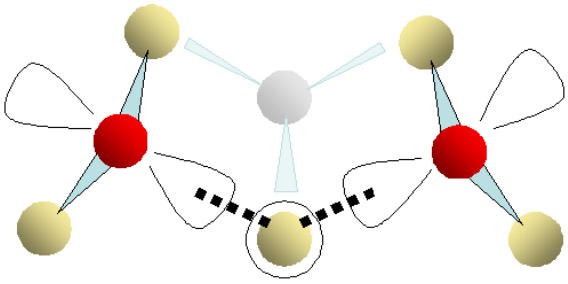

FIG. 14. Scheme of the inter-siloxane bridging in 2BR-B configuration. The empty circle around the central Si atom is a vertical hybrid AO.

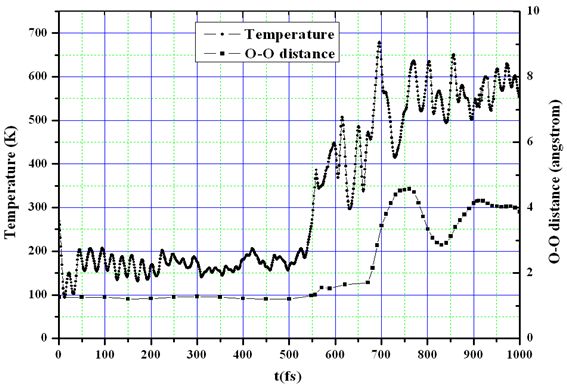

FIG. 15. Evolution of local temperature and O-O distance during FPMD simulation of the oxygen molecular chemisorption reaction.

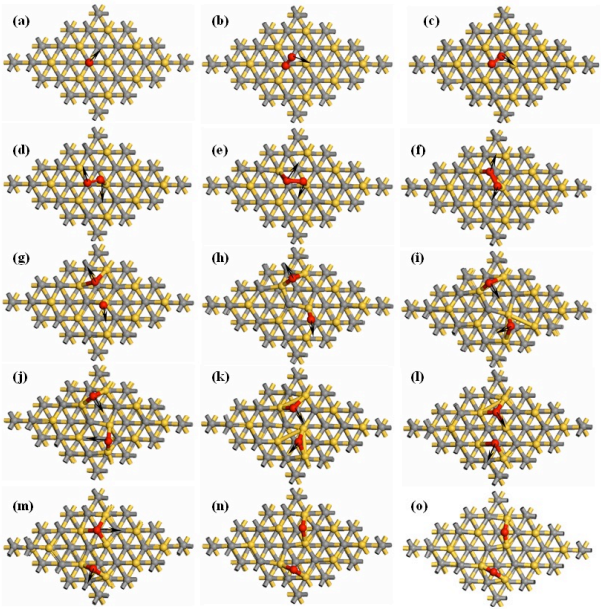

FIG. 16. Snapshots from FPMD simulation of the dissociative adsorption of molecular oxygen on the 3C-SiC(111) surface. The arrows indicate the moving directions of oxygen atoms. (a) Initial configuration (simulation time t=0); (b) t=200 fs; (c) t=500 fs; (d) t=500 fs; (d) t=556 fs; (e) t=587 fs; (f) t=665 fs; (g) t=685 fs; (h) t=725 fs; (i) t=745 fs; (j) t=767 fs; (k) t=805 fs; (l) t=845 fs; (m) t=875 fs; (n) t=916 fs; (o) final configuration t=1000 fs.

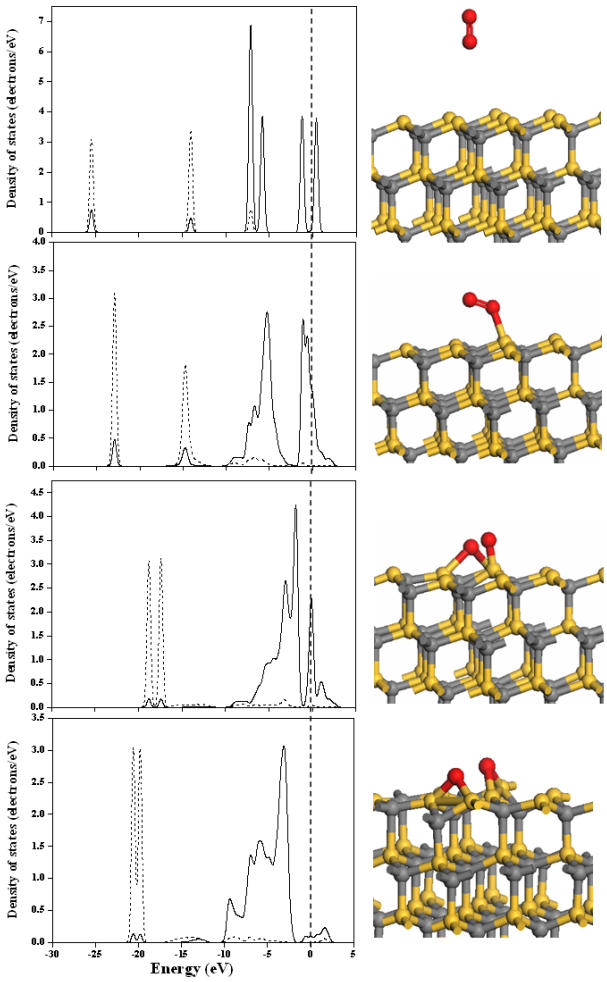

FIG. 17. Evolution of the local density of states projected onto the O atoms during the adsorption of molecular oxygen on 3C-SiC(111) surface (left) and correspondent snapshots (right) from a FPMD simulation started with the molecule perpendicular to the surface over a T4 site. The vertical line indicates the Fermi level. The continuous and dashed lines indicate the O 2s and 2p states, respectively, (a) Initial configuration (t=0 fs); (b) Adsorption (t=554 fs); (c) Dissociation (t=664 fs); (d) Final configuration (t=1000 fs)

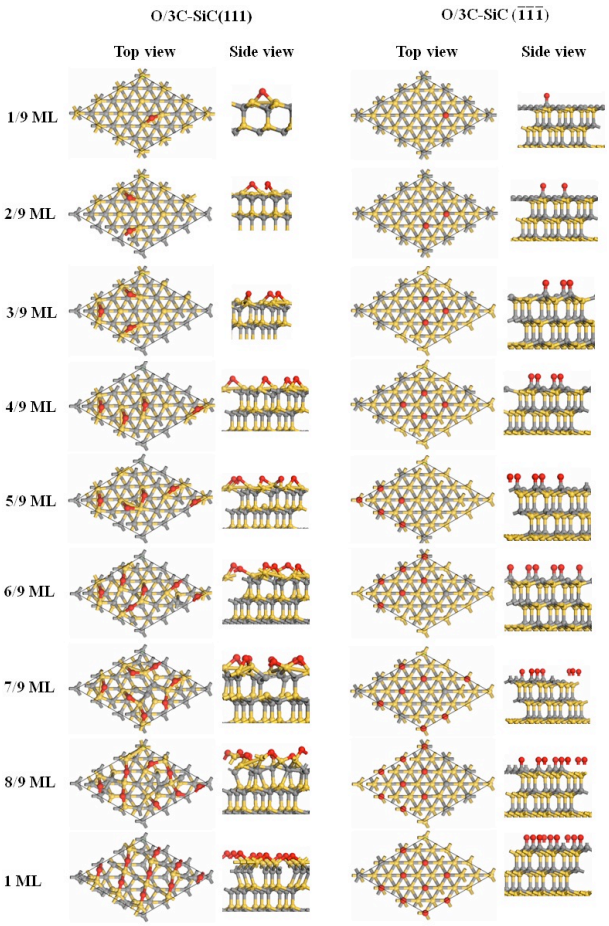

FIG. 18. Top and side view of optimized structures of O adsorption at the BR site of the 3C-SiC(111) surface and OT site of the 3C-SiC $(\bar{1}\bar{1}\bar{1})$ at various O coverages.

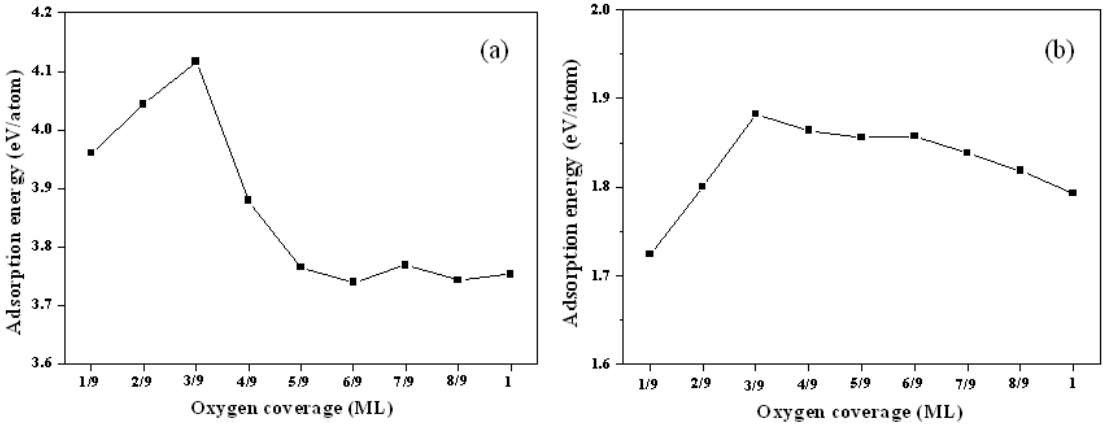

FIG. 19. Adsorption energies per oxygen adatom as a function of oxygen coverage. (a) Oxygen adsorptions on 3C-SiC(111) surface; (b) Oxygen adsorptions on 3C-SiC $(\bar{1}\bar{1}\bar{1})$ surface.

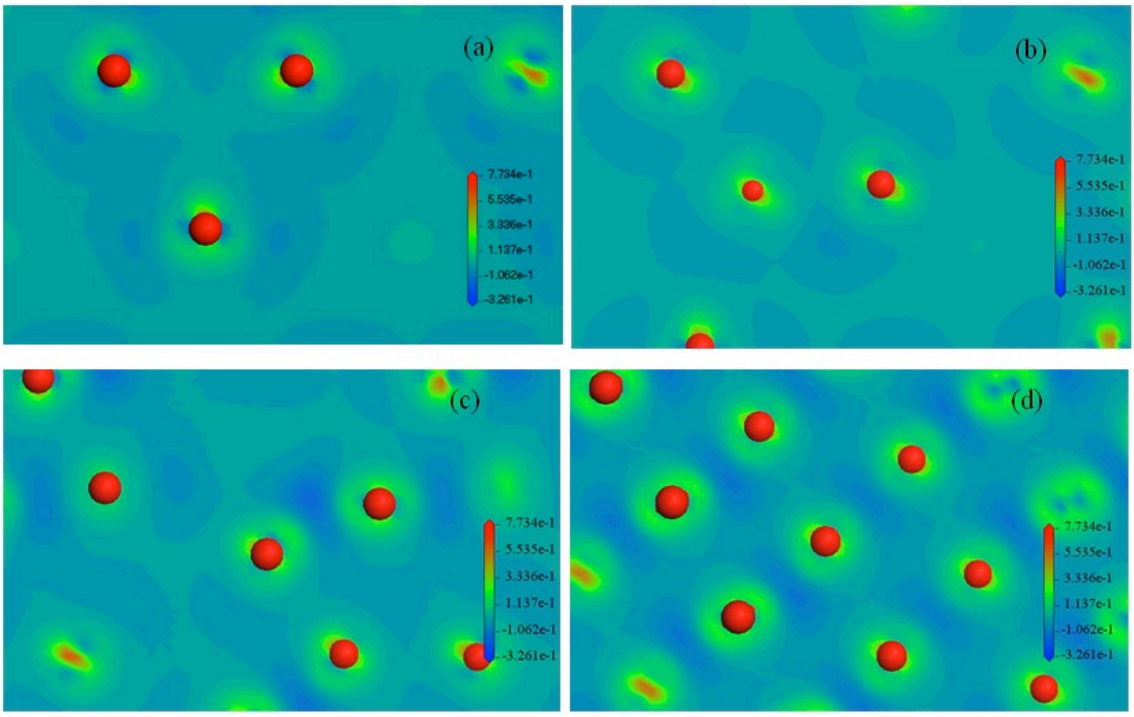

FIG. 20. Contour plot (through a plane containing the O adatoms marked in the figure and parallel to (111) surface) of difference electron densities for coverages of 3/9 (a), 4/9 (b), 6/9 (c), and 1.0 ML (d) on 3C-SiC(111) surface.

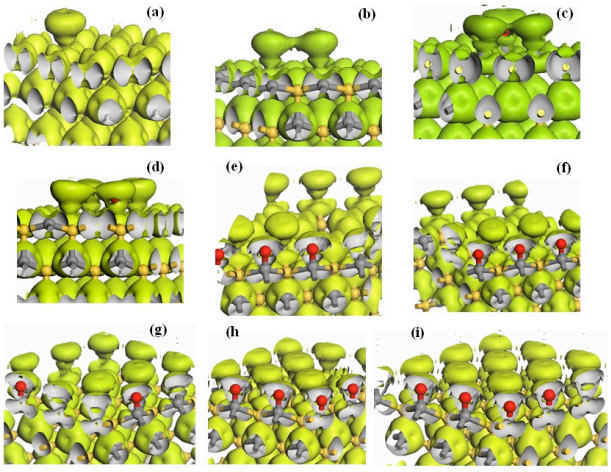

FIG. 21. Three-dimensional real-space contour plots of difference electron densities for O OT site on 3C-SiC $(\bar{1}\,\bar{1}\,\bar{1})$ for coverages of 1/9 (a), 2/9 (b), 3/9 (c), 4/9 (d), 5/9 (e), 6/9 (f), 7/9 (g), 8/9 (h) and 1.0 ML (i). The value of the isospheres of (a), (b), (d) and (d) are $1\times10^{-3}e$/ Å^3; the value of the isospheres of (e), (f), (g), (h) and (i) are $1\times10^{-5}e$/ Å^3.